Dirty quantum Hall ferromagnets and quantum Hall spin glasses

Derek K. K. Lee
Blackett Laboratory, Imperial College London, London SW7 2AZ, United Kingdom

Sebastian Rapsch and J. T. Chalker
Theoretical Physics, University of Oxford, 1 Keble Rd, Oxford OX1 3NP, United Kingdom

(Received 18 October 2002; published 20 May 2003)

We study quantum Hall ferromagnets in the presence of a random electrostatic impurity potential, within the framework of a classical nonlinear sigma model. We discuss the behavior of the system using a heuristic picture for the competition between exchange and screening, and test our conclusions with extensive numerical simulations. We obtain a phase diagram for the system as a function of disorder strength, Δ, and deviation, $\delta\nu$, of the average Landau-level filling factor from unity. Screening of an impurity potential requires distortions of the spin configuration. In the absence of Zeeman coupling there is a disorder-driven, zero-temperature phase transition from a ferromagnet at small Δ and $|\delta\nu|$ to a spin glass at larger Δ or $|\delta\nu|$. We characterize the spin-glass phase in terms of its magnetic and charge response.

DOI: 10.1103/PhysRevB.67.195322 PACS number(s): 73.43.Cd, 75.10.Nr, 71.10.−w

I. INTRODUCTION

Disorder and interactions have competing consequences in quantum Hall ferromagnets (QHFM's). In this paper, we study how a disordered impurity potential can give rise to a spin-disordered ground state. We also discuss the influence of disorder on the magnetic and charge response of such a system. We use a classical spin model throughout to describe the quantum Hall ferromagnet.

Coulomb interactions lead to spin correlations in a quantum Hall system. For electrons fully occupying the lowest Landau level (filling fraction $\nu=1$), exchange is responsible for a spin-polarized ground state, even in the absence of Zeeman energy. This is the consequence of Hund's rule as applied to a macroscopically large number of degenerate Landau-level orbitals. The resulting quantum Hall ferromagnet is especially interesting as a system in which the spin configuration and the charge density are closely linked.[1] At $\nu=1$ and if Zeeman energy is large, charge enters the spin-polarized system as minority-spin electrons. However, if Zeeman energy is small or vanishing, the charged excitation of lowest energy is not a bare spin-half electron, but a bound state of an electron with many spin waves. In classical terms, this occurs because the minority spin polarizes its local ferromagnetic background, and the composite object may be viewed as a topological excitation, or texture in an ordered ferromagnet — a skyrmion.[2] Similarly, an antiskyrmion, with topological charge of the opposite sign, is produced when charge is removed from a filled Landau level. In this description, the deviation of local charge density from that of a filled and ferromagnetically polarized Landau level is proportional to the topological density[3] of the spin configuration.

In a clean system with sufficiently small Zeeman energy, skyrmions or antiskyrmions can be created at zero temperature on varying the average filling factor from $\nu=1$ to larger or smaller values. For a disordered quantum Hall ferromagnet, the coupling of an electrostatic impurity potential to the charge density offers an additional mechanism by which spin textures are nucleated at zero temperature. The physical consequences of this coupling are the subject of this paper, which provides a detailed account of work presented in outline in Ref. 4.

The interplay between disorder and exchange in quantum Hall ferromagnets has been examined previously from several different viewpoints. Fogler and Shklovskii[5] developed a theory particularly applicable in higher Landau levels. Building on earlier discussions,[6] they presented a mean-field treatment in the spirit of Stoner theory. For odd integer filling in the absence of Zeeman coupling, they found a transition between ferromagnetic and paramagnetic ground states with increasing disorder strength. They suggested that this transition should be apparent in transport measurements, in which the ferromagnetic phase is characterized by spin-resolved Shubnikov–de Haas oscillations, and the paramagnet by spin-unresolved oscillations. Experimentally, a transition of this kind is observed with decreasing magnetic-field strength,[7,8] and its sharpness suggests that its origin is indeed cooperative.

Within the Fogler-Shklovskii approach, local moments are all collinear in the ferromagnet and vanish at the transition to the paramagnet. An alternative scenario may arise in the lowest Landau level near $\nu=1$, in which the QHFM responds to disorder mainly through the direction rather than the magnitude of its local magnetization. Some indications that this can happen derive from calculations for the fully polarized ferromagnet at weak disorder. Here, a reduction in spin stiffness with increasing disorder strength has been interpreted by Green[9] as a precursor of a noncollinear phase. Moreover, even weak disorder may nucleate a dilute glass of skyrmions and antiskyrmions at the maxima and minima of the disordered potential, as discussed by Nederveen and Nazarov[10] and examined further in the present paper. In addition, Sinova, MacDonald, and Girvin[11] have shown that, at intermediate disorder strength, both reduced and noncollinear local moments emerge from a numerical solution of Hartree-Fock theory for a model with Coulomb interactions and spatially uncorrelated disorder, while transport properties

within Hartree-Fock theory have been discussed by Murthy.[12]

In general, we believe that the relative importance of local-moment reduction versus the formation of spin textures for dirty QHFM's will depend on the nature of the disorder. In this work, we concentrate on textures, which are favored by a smoothly varying impurity potential at $\nu=1$. We find that the ferromagnet gives way to a spin glass at strong disorder.

The plan of this paper is as follows. In the next section, we describe a spin model with quenched disorder which is intended to capture the physics of the disordered QHFM. This is followed in Sec. III by a discussion of the phase diagram for the model as a function of filling factor and disorder strength, using heuristic arguments and scaling ideas. The conclusions are supported by the results of a Monte Carlo simulation of a lattice version of the spin model. The technique is outlined in Sec. IV and the results are presented in Sec. V. In Secs. VI and VII, we discuss the compressibility and conductivity of the system in order to characterize the charge response of spin-disordered ground states.

II. SPIN MODEL

Consider a two-dimensional electron gas in a strong perpendicular magnetic field B, with Landau-level filling ν close to unity. The electrons are subject to an impurity potential $V(\mathbf{r})$ and an electron-electron interaction energy $U(\mathbf{r})$. As a first step, let us omit the exchange interactions and the Zeeman energy. Then the electron density $\rho(\mathbf{r})$ is determined by the balance between disorder and interactions, or in other words, screening. We treat this using Thomas-Fermi theory. Such an approximation has been applied by Efros[13,14] to the comparable problem in spin-polarized Landau levels when ν lies near half-integer values. The ground-state charge density $\rho(\mathbf{r})$ at weak disorder is determined by the condition that the Hartree potential should match the chemical potential μ everywhere:

$$\mu = V(\mathbf{r}) + \int U(\mathbf{r}-\mathbf{r}')\rho(\mathbf{r}')d^2\mathbf{r}'. \tag{1}$$

This approach is valid in the case where the resulting local filling factor varies smoothly on the scale of the magnetic length, $l_B=(\hbar/eB)^{1/2}$, and only has small fractional deviations from $\nu=1$, so that

$$\delta\rho(\mathbf{r}) \equiv \rho(\mathbf{r}) - (2\pi l_B^2)^{-1} \ll \rho(\mathbf{r}). \tag{2}$$

However, the Thomas-Fermi picture of good local screening does not take into account exchange interactions. Provided that electron-density fluctuations are small and smoothly varying, ferromagnetic exchange leads locally to a maximal ferromagnetic polarization of the electron spins. This local magnetization may vary in space. Denoting its direction by the three-component unit vector $\vec{S}(\mathbf{r})$, spatial fluctuations in spin orientation are linked to electron density by[2,3]

$$\delta\rho(\mathbf{r}) = \frac{1}{8\pi}\epsilon_{ij}\vec{S}\cdot(\partial_i\vec{S}\times\partial_j\vec{S}). \tag{3}$$

This direct connection is specific to the quantum Hall ferromagnet — a varying electron density implies a variation in the direction of the local magnetization and vice versa. Such spin textures cost exchange energy. So, a proper description of the system must include exchange, impurity, and Hartree contributions to the total energy of a dirty quantum Hall ferromagnet. This brings us to study the Hamiltonian

$$\mathcal{H} = \int \left\{ \frac{J}{2}|\nabla\vec{S}(\mathbf{r})|^2 + [V(\mathbf{r})-\mu]\delta\rho(\mathbf{r}) + \frac{U_0}{2}[\delta\rho(\mathbf{r})]^2 \right\} d^2\mathbf{r}, \tag{4}$$

where

$$J = \frac{1}{16(2\pi)^{1/2}} \frac{e^2}{4\pi\epsilon_0\epsilon_r l_B} \tag{5}$$

is the exchange coupling.[15] (ϵ_r is the relative permittivity in the semiconductor.) At this point we have chosen for simplicity a short-range Hartree interaction, $U(\mathbf{r}-\mathbf{r}')=U_0\delta(\mathbf{r}-\mathbf{r}')$. We have also absorbed the constant $U_0/2\pi l_B^2$ into the chemical potential μ.

As mentioned above, we work with a disordered potential $V(\mathbf{r})$ that is smooth on the scale of the magnetic length l_B. For simplicity, our discussion of this continuum model assumes a Gaussian distribution with standard deviation Δ and correlation length λ much larger than the magnetic length l_B. (Our numerical study uses a lattice model with a bounded distribution with uncorrelated disorder.)

In restricting our study to this model, we neglect quantum fluctuations of $\vec{S}(\mathbf{r})$. This semiclassical approximation is justified for smooth variations, with $|\nabla\vec{S}(\mathbf{r})| \ll l_B^{-1}$. Our aim in the following is to understand the zero-temperature phase diagram of the model defined by Eq. (4), as a function of disorder strength Δ and average charge density $\langle\delta\rho\rangle$, the spatial average of $\delta\rho(\mathbf{r})$. We will characterize its ground states via their response functions and excitations.

We conclude this section by comparing this model with some other examples of disordered systems. As an electron system, it is unusual in that there is an exchange gap for single-particle excitations, even if the ground-state spin configuration $\vec{S}(\mathbf{r})$ does not have long-range ferromagnetic order. This means that the only low-energy excitations involve collective spin modes. As a ferromagnet with quenched disorder, the system is also unusual in several ways. First, the link between spin and charge means that the spin system responds to applied electric fields. We calculate in the following the wave-vector-dependent dielectric constant, $\epsilon(q)$, and compare it with behavior found in more conventional disordered electron systems. Second, due to the same coupling, spin waves generate an electric dipole moment. This means that spin waves contribute to the optical conductivity $\sigma(\omega)$. More generally, the coupling to disorder in this model leaves spin-rotational symmetry intact but breaks time-reversal symmetry. This is in contrast to the effect of random

Zeeman fields, which break both symmetries, and to random exchange interactions, which preserve both symmetries.

III. PHASE DIAGRAM

We begin with a qualitative discussion of the zero-temperature phase diagram as a function of disorder strength and average charge density. We employ scaling arguments to obtain the phase boundary for breakdown of long-range ferromagnetic order.

The Hamiltonian of Eq. (4) for the continuum model is minimized by the spin configuration which satisfies (Appendix A)

$$J\nabla^2\vec{S}\times\vec{S}=\epsilon_{ij}\partial_i V_{\mathrm{H}}(\mathbf{r})\partial_j\vec{S}, \tag{6}$$

$$V_{\mathrm{H}}(\mathbf{r})=V(\mathbf{r})-\mu+U_0\delta\rho(\mathbf{r}), \tag{7}$$

where V_{H} the local Hartree potential and $\delta\rho$ is defined in terms of the local spin configuration by Eq. (3). This equation for the ground-state configuration shows the interplay between exchange and disorder in the model. Since it is difficult to tackle the nonlinear equation directly, we proceed using heuristic arguments instead.

The model is characterized by two energy scales: the exchange energy J and the disorder strength Δ. There are also two length scales: the correlation length λ of the disordered potential and

$$L_{\mathrm{H}}\equiv(U_0/J)^{1/2}, \tag{8}$$

which we call the Hartree length. The significance of the Hartree length can be made clear by considering a skyrmion of fixed shape and radius R in a clean system. The contribution to its total energy from exchange is $\sim J$, independent of size, while that from Hartree interactions is size dependent, being $\sim U_0/R^2$. Comparing these contributions, one sees that exchange dominates on length scales large compared with L_{H}, while Hartree interactions dominate at smaller distances.

Our central hypothesis is that the competition between interaction and disorder in this system is characterized by the Hartree length only. In the following, we also use the limit $L_{\mathrm{H}}\gg\lambda$ as a source of simplifications.

A. Filled Landau level

Let us consider first the effect of disorder on a system at $\nu=1$, imposed by setting $\langle\delta\rho\rangle=0$. Without impurities $[V(\mathbf{r})=0]$, the system is a perfect ferromagnet. Moreover, there is a threshold[9–11]

$$|V(\mathbf{r})|=4\pi J, \tag{9}$$

below which an impurity potential is unscreened. It arises because, for any $\vec{S}(\mathbf{r})$, one has $|\nabla\vec{S}(\mathbf{r})|^2\geq 8\pi|\delta\rho(\mathbf{r})|$ and hence

$$\mathcal{H}\geq\int[4\pi J|\delta\rho(\mathbf{r})|+V(\mathbf{r})\delta\rho(\mathbf{r})]d^2\mathbf{r}. \tag{10}$$

Thus, if $|V(\mathbf{r})|$ is below the threshold $4\pi J$ everywhere, the ground state is the perfectly aligned ferromagnet with $\delta\rho(\mathbf{r})=0$.

At weak disorder ($\Delta\lesssim J$), $|V(\mathbf{r})|$ in most parts of the system lies below the threshold. With an unbounded potential distribution, the ground-state spin configuration therefore consists of a dilute glass of skyrmions and antiskyrmions, nucleated at rare positions where $|V(\mathbf{r})|$ is large, as discussed by Nederveen and Nazarov.[10] Away from these positions we expect that the ferromagnetic order is essentially unaffected by the impurity potential. A careful treatment of this regime is, however, quite subtle, since the spin deviation due to an isolated skyrmion falls off with distance only as r^{-1}. We argue in Appendix C that long-range ferromagnetic order is indeed preserved, and that the internal degrees of freedom of dilute skyrmions and antiskyrmions develop the correlations necessary to ensure this.

In contrast, at strong disorder ($\Delta\gg J$), the charge density provides almost perfect local screening of the disordered potential, so that

$$\delta\rho(\mathbf{r})\simeq -V(\mathbf{r})/U_0 \quad (\Delta/J\gg 1). \tag{11}$$

Corrections to perfect Thomas-Fermi screening arise at length scales larger than L_{H}, where exchange becomes important. The effect of exchange is to force screening charges to be quantized, since an unquantized charge costs divergent exchange energy in the thermodynamic limit. We can summarize the effect of exchange by dividing the system into regions of area L_{H}^2, finding for each such area the integral

$$Q\equiv-\int_{L_{\mathrm{H}}^2}\frac{V(\mathbf{r})}{U_0}d^2\mathbf{r} \tag{12}$$

and adjusting the total screening charge within every region to the integer value closest to Q. We argue that these integers are predominantly zero in a ferromagnetic phase, and predominantly nonzero in a phase without ferromagnetic order. To illustrate this, we consider a well-ordered ferromagnetic phase, in which $S(\mathbf{r})$ has small spatial variations around a global direction of magnetization. In this case, the net topological charge in any region has a magnitude much less than one. Conversely, in a phase without such order, unit topological charge will typically accumulate over a region of linear size given by the ferromagnetic correlation length.

This picture leads us to identify the phase boundary of the ferromagnet as the point at which $\langle Q^2\rangle^{1/2}\sim 1$. To estimate $\langle Q^2\rangle$, we note from Eq. (12) that each correlation area of size λ^2 contributes to Q a charge of magnitude $\lambda^2\Delta/U_0$ and a random sign. Over the Hartree area, there are $L_{\mathrm{H}}^2/\lambda^2$ such contributions, so that

$$\langle Q^2\rangle^{1/2}\sim(\lambda^2\Delta/U_0)(L_{\mathrm{H}}/\lambda)=\lambda L_{\mathrm{H}}\Delta/U_0. \tag{13}$$

The phase boundary is therefore given by

$$\Delta_c\sim U_0/(\lambda L_{\mathrm{H}})=J(L_{\mathrm{H}}/\lambda). \tag{14}$$

For $\Delta>\Delta_c$, the ground state is strongly disordered and has no ferromagnetic order. Within our classical description, the

spins are frozen at zero temperature. We can therefore identify this phase as a quantum Hall spin glass.

B. Away from integer filling

We consider next the ground state away from $\nu=1$. We examine behavior at fixed $\Delta<\Delta_c$, as a function of the average charge density $\langle\delta\rho\rangle\propto\nu-1$. For $\langle\delta\rho\rangle=0$ and $\Delta<\Delta_c$, the system has a net magnetization, but the introduction of charge in the form of skyrmions (or antiskyrmions) disrupts ferromagnetic spin alignment. The size R of an isolated skyrmion in a clean system is divergent if Hartree repulsion is not balanced by Zeeman energy. However, the presence of an impurity potential establishes an optimal size, because it is energetically favorable for a skyrmion to locate its charge distribution in randomly occurring potential wells. The typical depth of such a well of radius $R\gg\lambda$, averaged over its area, is $-\Delta(\lambda/R)$. (The case $\lambda>R$ is treated in Ref. 10.) The Hartree energy is $\sim U_0/R^2$. The total energy is hence minimized if

$$R\sim U_0/(\Delta\lambda)=L_{\mathrm{H}}(\Delta_c/\Delta). \tag{15}$$

Note that this value of R exceeds L_{H} for $\Delta<\Delta_c$. Because of this, we expect that exchange energy dominates over the potential energy and that the skyrmion will not be strongly distorted by the random potential. In other words, screening as discussed in the previous subsection does not alter the present argument.

We expect that ferromagnetic order will persist with increasing charge density until such skyrmions overlap. The phase boundary hence lies at

$$\langle\delta\rho\rangle_c=L_{\mathrm{H}}^{-2}(\Delta/\Delta_c)^2. \tag{16}$$

In summary, we have used simple arguments to obtain the phase boundaries between the ferromagnetic and the spin glass as a function of disorder and charge density. The results, Eqs. (14) and (16), are summarized in the schematic phase diagram shown in the inset of Fig. 3 below. We next present results from Monte Carlo simulations which support these predictions.

The discussion we have presented is for a model with a short-range Hartree interaction and for the limit $l_B\ll\lambda\ll L_{\mathrm{H}}$. The central consequence of using a Coulomb form, $U(r)=e^2/4\pi\epsilon_0 r$, in place of a short-range Hartree interaction is to change the length scale derived by comparing Hartree with exchange energies, from $L_{\mathrm{H}}\equiv(U_0/J)^{1/2}$ to $L_{\mathrm{H}}\equiv e^2/4\pi\epsilon_0 J=16(2\pi)^{1/2}l_B$. Since in this case L_{H} is not parametrically larger than l_B, scaling arguments of the type presented in this section are not justified. In this case, in place of three distinct regimes of disorder strength ($\Delta\ll J$, $J\ll\Delta\ll\Delta_c$ and $\Delta_c\ll\Delta$) we expect only two, with $\Delta_c\sim J$. We note that the differences in behavior resulting in a short-range Hartree interaction or from a Coulomb form are likely to be largest when $\delta\nu$ and Δ are small (in the lower left corner of Fig. 3 below), where screening is weakest.

We expect that thermal fluctuations at nonzero temperature will disorder both the ferromagnet and the spin glass, albeit with a long correlation length at low temperature. Thermal disorder for the clean ferromagnet has been discussed, in Refs. 16 and 17.

IV. MONTE CARLO SIMULATIONS

In order to test the theoretical results derived in the previous section, we use Monte Carlo methods, in combination with simulated annealing, to study a classical Heisenberg model with quenched disorder. In this section, we outline our methodology. Similar techniques have been applied recently to systems without quenched disorder, in Ref. 18. We present our results for the physical response functions of the model in Secs. V and VI.

We treat a lattice version of Eq. (4) with $N\times N$ classical spins $\vec{S}_i$ of unit length on a square lattice, taking periodic boundary conditions. Spins have nearest-neighbor ferromagnetic interactions of strength J. In addition, the electrical charge q_k on each plaquette k is calculated from the area on the spin sphere covered by the spins on the corners of that plaquette. This charge density has a local repulsive Hartree interaction of strength U_0, and is also subject to a uniformly distributed random background potential $\epsilon_k\in[-\Delta,\Delta]$. Since we choose this potential independently for each plaquette, the correlation length λ is set by the lattice spacing.

The Hamiltonian of the lattice model is

$$H=-J\sum_{\langle ij\rangle}\vec{S}_i\cdot\vec{S}_j+\sum_k\left(\epsilon_k q_k+\frac{U_0}{2}q_k^2\right)+\gamma\left(Q_0-\sum_k q_k\right)^2, \tag{17}$$

where we have introduced a Lagrange multiplier γ to bias the system towards a predefined number Q_0 of charge quanta.

To obtain the ground-state spin configuration for a given disorder realization, we start from a random initial state and anneal using Monte Carlo dynamics and the Metropolis algorithm. After some experimentation, we found the following three-stage protocol to be effective. In the first stage, the temperature is reduced linearly in time from a high temperature T_0 (several times J) to $T_0/10$, using 3.5×10^5 Monte Carlo steps per spin (MCS). In the second stage, the temperature is reduced from $T_0/10$ to 0, using 5×10^5 MCS. For both these stages, the attempted spin update is an isotropically distributed reorientation. In the third stage, the system is quenched for a further 5×10^4 MCS, using as the attempted spin update only small-angle reorientations in order to improve the acceptance rate.

We have checked that this algorithm finds the ground state reliably for a weakly disordered system with overall charge neutrality, by doing repeated runs for a given realization of background potential and using local charge and energy densities to identify states that differ only by a global spin rotation. In strongly disordered systems and those with nonzero average charge density, repeated applications of the algorithm do not reproduce the same state to high precision. Instead, a number of low-lying states are obtained, having a small spread (less than 10%) in their energies and other ob-

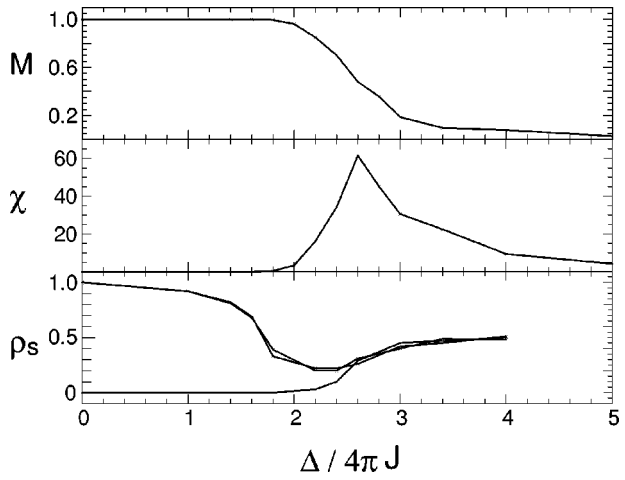

FIG. 1. Ground-state properties for a system with $U_0=8\pi J$ as a function of disorder strength (Ref. 4): (a) magnetization M as a fraction of the saturated moment, (b) susceptibility χ, and (c) spin stiffness ρ_s in units of J.

servables such as their magnetization. We performed at least five independent simulations for every disorder realization and picked from the states obtained the one with the lowest energy. For a chosen disorder strength Δ, we generated three or more realizations of the disorder potential and averaged our results over these realizations. We found that properties such as the ground-state energy, the magnetization and various response functions show only small fluctuations between different disorder realizations for systems of size 32×32 spins or larger. Simulations of much larger systems are ruled out by constraints on computing time, and we choose $N=40$ as the system size for most of our simulations.

The Lagrange multiplier γ was chosen sufficiently large so that a majority of the simulation runs yielded a ground state with the desired total charge Q_0. We do not detect any dependence of our results on the particular value of γ.

V. MAGNETIC RESPONSE

Having outlined our simulation techniques, we next present our results. We start with the magnetic properties of the system. We show that they indicate a transition from the ferromagnet to the spin glass with increasing disorder strength, as expected from our discussions in Sec. III.

A. Magnetization

We calculate the site-averaged magnetization

$$M=|\langle \vec{S}(\mathbf{r})\rangle| = N^{-2}\left|\sum_i \vec{S}_i\right|. \tag{18}$$

Results are shown for a system of 40×40 spins with $U_0=8\pi J$ in Fig. 1(a). Spins are fully aligned for $\Delta/4\pi J<1$, because our bounded disorder distribution then lies entirely below the threshold, Eq. (9). Increasing Δ beyond $4\pi J$, we obtain a partially polarized ferromagnet. In fact, the magnetization remains close to its saturated value until $\Delta/4\pi J \simeq 1.8$, when it starts to drop appreciably. Increasing the disorder strength further, we reach a regime of strong disorder at $\Delta/4\pi J\simeq 3$, in which there is only a small magnetization, of the magnitude expected for a spin-glass state of a finite-size system.

These results are consistent with the existence of a phase transition from the collinear, ordered phase at weak Δ to a spin-glass phase at strong disorder. From the magnetization curve we pick $\Delta_c/4\pi J\simeq 2.5$ as our estimate of the critical disorder strength.

B. Susceptibility

We also calculate the uniform susceptibility χ from the response of the ground state to a weak Zeeman field. Our procedure is as follows. First we obtain a ground state without a Zeeman field, using the protocol described in Sec. IV. Then we apply a weak Zeeman field $\vec{h}$ in the direction of the residual magnetization, by adding to the Hamiltonian the perturbation $\delta H=-\vec{h}\cdot\vec{M}$. We find the ground state in the presence of this perturbation by repeating the third stage of the quenching protocol. Taking care to check that our measurements remain within the linear response regime, we extract the susceptibility from the change in the magnetization $\delta\vec{M}$, using

$$\chi=|\delta\vec{M}|/|\vec{h}|. \tag{19}$$

Results for $U_0=8\pi J$ are shown in Fig. 1(b). The susceptibility as a function of disorder strength has a large peak at $\Delta/4\pi J=2.5$. We interpret this as a second indication of a phase transition from the ferromagnetic phase to a disordered phase.

C. Spin stiffness

We now turn to the spin stiffness ρ_s which measures the rigidity of the spin configuration. It is obtained by calculating the energy cost of small amplitude, long-wavelength spin twists in the ground state. More specifically, we label the columns of sites in the $N\times N$ lattice by integers $1,2,\ldots,N$. Then, starting with a ground state obtained as in Sec. IV, we construct a twisted state by rotating all spins on column $N/2$ of the system through a small angle θ about an axis $\vec{e}$. Using the third stage of the quenching protocol, we then relax all spins in this twisted state except those on columns 1 and $N/2$, which are held fixed. From the difference in energy ΔE between the initial and final states, we obtain the spin stiffness for rotations about the axis $\vec{e}$, using

$$\rho_s=\Delta E/2\theta^2. \tag{20}$$

Repeating this for different axes of rotation, we calculate the full 3×3 symmetric tensor for the spin stiffness, $\rho_s^{\alpha\beta}$. As expected, in the ferromagnetically ordered phase one of the principal axes of this tensor lies to a good approximation along the magnetization direction, and it is convenient in these calculations to choose rotation axes $\vec{e}$ in directions parallel and perpendicular to $\vec{M}$.

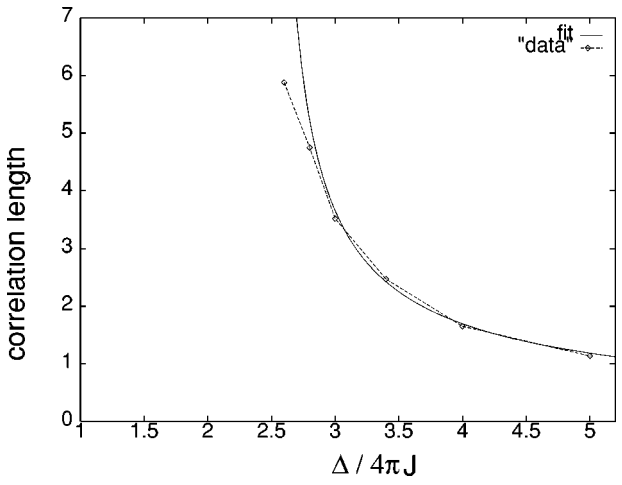

FIG. 2. Correlation length (in units of the lattice constant) as a function of the disorder strength. Open symbols: our calculation; solid line: fit to a power law.

The eigenvalues of the spin stiffness tensor are shown as a function of disorder strength in Fig. 1(c). For the fully polarized ferromagnet, rotations about the magnetization direction do not alter the spin configuration, and so one eigenvalue is zero while the other two are degenerate, taking the value $\rho_s = J$. For the partially polarized ferromagnet, all three eigenvalues are nonzero, with two remaining degenerate. The spin-glass state, however, has no special spin direction and this magnetic isotropy means that that all three eigenvalues are approximately degenerate. The stiffness is reduced in value from J in the fully polarized ferromagnet to approximately $J/2$ in the spin glass. (A variational estimate for the stiffness in the spin-glass phase is $2J/3$. See Appendix A.) The magnetically isotropic phase is observed for $\Delta/4\pi J > 2.5$, yielding the same estimate of Δ_c as our magnetization and susceptibility data.

D. Spin-correlation length

The behavior of spin correlations provides a further way of characterizing ground states. In particular, we consider the correlation function

$$C(r) = \frac{1}{N_r} \sum_{(r)} \vec{S}_i \cdot \vec{S}_j , \tag{21}$$

where the sum runs over all N_r spin pairs of separation r. We extract the spin correlation length ξ by fitting to the form

$$C'(r) = M^2 + (1 - M^2)\exp(-r/\xi). \tag{22}$$

The behavior of the correlation length as a function of the disorder strength in the spin-glass phase is shown in Fig. 2. From the Harris criterion,[19] we expect it to diverge as $\xi \sim (\Delta - \Delta_c)^{-\nu}$ with $\nu > 2/d = 1$ as the ferromagnetic phase boundary is approached. Our results are consistent with a divergence at $\Delta/4\pi J = 2.5$, although it appears that they are affected by finite-size effects for ξ for $\Delta/4\pi J < 2.7$. Perhaps because of these finite-size effects, this fit gives a low value for the exponent: $\nu = 0.7$. Attempts at a similar fit in the ferromagnetic phase are unsuccessful, and indeed the arguments of Appendix C suggest that correlations in this case may decay with a power law.

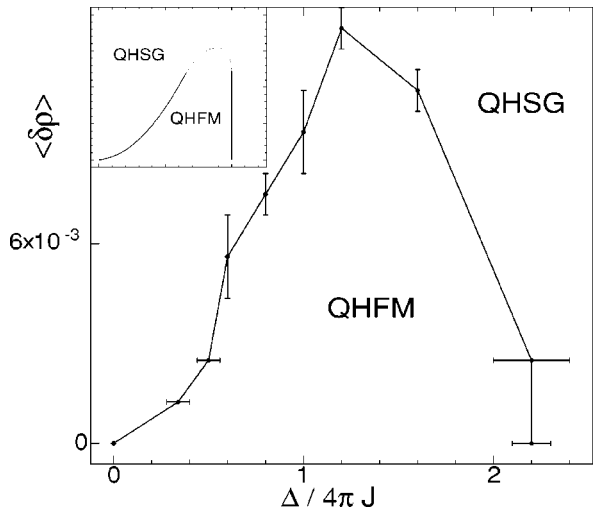

FIG. 3. The phase diagram for $U_0 = 4\pi J$ ($L_H/\lambda = \sqrt{4\pi}$), as a function of disorder strength and charge density. QHFM: quantum Hall ferromagnet; QHSG: quantum Hall spin glass. Inset: results from scaling arguments for $L_H/\lambda \gg 1$.

E. Phase diagram

Our Monte Carlo results outlined above allow us to distinguish between a ferromagnetic phase and a quantum Hall spin glass. For a system with $U_0 = 8\pi J$, we conclude that a phase transition from a collinear ferromagnet to a spin-disordered phase occurs at $\Delta/4\pi J = 2.5$. Repeating these calculations for different disorder strengths and charge densities, we can map out a phase diagram for the ground state of the system. Results for $U_0 = 4\pi J$ are shown in Fig. 3.

Comparing this with the phase diagram predicted from our heuristic arguments (inset), we see that the two are qualitatively very similar, even though the simulations are carried out for $(L_H/\lambda) = \sqrt{4\pi}$ while our scaling picture applies in the limit $(L_H/\lambda) \gg 1$. An idea of the dependence on L_H/λ is given by contrasting results at the two values of U_0 studied. The critical disorder Δ_c at which the neutral system loses ferromagnetic order is $\Delta_c/4\pi J \simeq 2.5$ for $U_0 = 8\pi J$, and reduces to $\Delta_c/4\pi J \simeq 2.2$ for $U_0 = 4\pi J$, in qualitative agreement with the scaling behavior we expect from Eq. (14).

It is interesting to note that there is a density range over which disorder may *stabilize* the ferromagnet, by limiting the size of the nucleated spin textures. This range is, however, very narrow: $|\langle \delta\rho \rangle| \lesssim 10^{-2}$ in units of charge per plaquette. We mention in passing that we have not searched extensively for a skyrmion crystal, expected at a finite charge density in the weak disorder limit but presumably unstable for $\Delta \neq 0$.

VI. DIELECTRIC RESPONSE

We have so far discussed the phase diagram of the system in terms of its magnetic correlations and response. We next study its charge response.

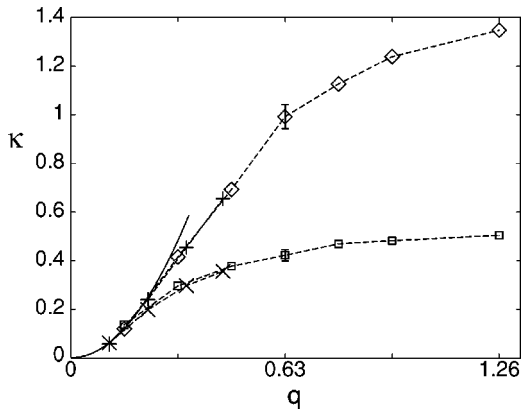

FIG. 4. Compressibility (Ref. 4) $\kappa(q)$ as a function of wave vector q for systems with $J=1$ and $U_0=4\pi$ and 8π. ($\Delta/4\pi J=3$, $\langle\delta\rho\rangle=0$.)

We examine first the dielectric response of the partially polarized ferromagnet and spin glass, characterized at zero frequency by the wave-vector-dependent dielectric constant $\epsilon(q)$ or by the compressibility $\kappa(q)$, related via

$$\kappa(q)=q^2\epsilon(q)\epsilon_0/e^2, \tag{23}$$

where e is the electron charge and ϵ_0 is the permittivity of the medium. More precisely, we apply a periodic modulation, $V(\mathbf{r})\rightarrow V(\mathbf{r})+V_1\cos(\mathbf{q}\cdot\mathbf{r})$, to the potential in Eq. (4). As a result, the ground-state electron density changes according to $\delta\rho(\mathbf{r})\rightarrow\delta\rho(\mathbf{r})+\delta\rho_1(\mathbf{r})$. Since the system is disordered, $\delta\rho_1(\mathbf{r})$ contains many Fourier components, but after averaging, the linear response is

$$\langle\delta\rho_1(\mathbf{r})\rangle=-V_1\kappa(q)\cos(\mathbf{q}\cdot\mathbf{r}), \tag{24}$$

which constitutes our definition of $\kappa(q)$.

Our numerical results for $\kappa(q)$ are displayed in Fig. 4, where we study systems deep in the spin-glass phase, setting $\Delta/4\pi J=3$ and $\langle\delta\rho(\mathbf{r})\rangle=0$. We compare behaviors at $U_0/4\pi J=1$ and at $U_0/4\pi J=2$, in each case combining data from lattices of size 40^2 and 56^2 in order to maximize wave-vector resolution.

We find that, at small q, $\kappa(q)$ is independent of U_0 and quadratic in q. At large q, it is independent of q, varying roughly as U_0^{-1}. We can understand these results for $\kappa(q)$ using the approach we employed to discuss the phase diagram. The Hartree length L_{H} again plays an important role.

For $q\gg L_{\mathrm{H}}^{-1}$, exchange may be neglected and we see from Eq. (12) that

$$\kappa(q)\simeq U_0^{-1}\quad(qL_H\gg1), \tag{25}$$

in agreement with the q-independent value obtained for $\kappa(q)$ at large wave vectors from our simulations, and with the U_0 dependence of these values.

Exchange becomes important at longer wave lengths $q\ll L_{\mathrm{H}}^{-1}$. To estimate $\langle\delta\rho_1(\mathbf{r})\rangle$ for small q, we suppose that it arises primarily from spin rotations which have amplitude $\delta\theta$ and wave vector $\sim\mathbf{q}$. To be specific, consider for the periodic perturbation $V_1\cos(qx)$ a region of size $2L\times L$ with $L=\pi/q$. The perturbation causes a net movement of charge

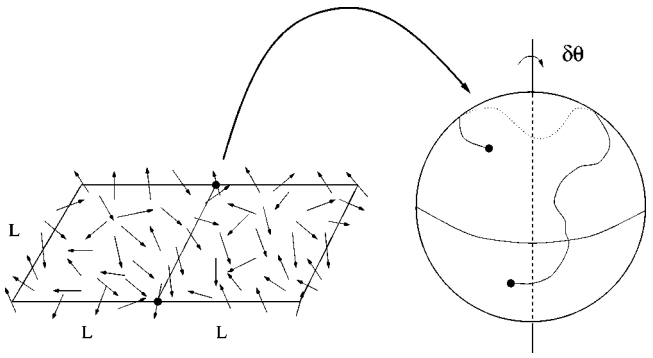

FIG. 5. Mapping a line of spins on the lattice to a trajectory in spin space.

δQ_1 in the x direction, from one side of this region to the other. We choose to focus on those spins lying on the line of length L which is parallel to the y axis and which divides the region into two equal halves of size $L\times L$. (See Fig. 5.) We suppose, in a variational spirit, that the charge movement induced by the perturbation involves simply a rigid rotation of these spins, through an angle $\delta\theta$. With this assumption, let us estimate the charge transfer generated by such a rotation, and the exchange energy that it costs. To do so, it is useful to regard the spin configuration as a map of the line we have defined onto a trajectory on the spin sphere. For a disordered spin configuration, this trajectory resembles a random walk. The end points of the walk are randomly placed on the spin sphere if L is large compared to the spin-correlation length ξ, and the distance D between them on the surface of the spin sphere is therefore typically $\mathcal{O}(1)$. Under a rigid rotation of spins on the line, the trajectory is displaced rigidly around the spin sphere. The charge transferred across the real-space line is proportional to the area swept out on the spin sphere by the trajectory during this displacement. We therefore arrive at the estimate

$$\delta Q_1\sim D\,\delta\theta\sim\delta\theta. \tag{26}$$

Choosing the phase and axis of rotation appropriately in each such region, the change in potential-energy density arising from the rotation is $-V_1\delta Q_1/L^2=-V_1q^2\delta\theta$ while the associated change in exchange energy density is $Jq^2\delta\theta^2$. Choosing $\delta\theta$ to minimize the total energy, we find $|\delta\rho_1(\mathbf{r})|\sim V_1q^2/J$ and hence

$$\kappa(q)\sim q^2/J=U_0^{-1}(qL_{\mathrm{H}})^2\quad(qL_{\mathrm{H}}\ll1). \tag{27}$$

This conclusion is again consistent with our numerical results.

Alternatively, we can arrive at this form for the compressibility from scaling considerations. In general, we may expect that the compressibility is described by the scaling form

$$\kappa(q)=U_0^{-1}f(qL_{\mathrm{H}}), \tag{28}$$

where $f(x)$ approaches a constant at large x. Our central hypothesis is that exchange dominates at small wave vectors, and so $\kappa(q)$ should be independent of U_0 as $q\rightarrow0$. This

implies that $f(x) \sim x^2$ for $x \ll 1$, leading to the form given in Eq. (27) for the compressibility at small q.

To summarize, the system has a metallic response to a perturbing potential at large wave vectors, with $\kappa(q)$ independent of q. However, at small wave vectors, it behaves like an insulator, with $\epsilon(q)$ independent of q.

We note that, for an infinite system at exactly $q=0$ and zero frequency, $\kappa(0)$ should be proportional to the thermodynamic density of states. So, except in the fully polarized ferromagnet, we expect that $\kappa(0)$ remains finite as we take the temperature to zero. To reconcile this general expectation with our results, one must remember that for finite-size systems considered here at zero temperature, the discreteness of charge implies that almost all disorder realizations have no response to an infinitesimal change in the chemical potential, while there is a divergent response from those realisations for which ground states from two different charge sectors are degenerate.

VII. OPTICAL CONDUCTIVITY

Finally, we consider the optical conductivity $\sigma(\omega)$ at frequency ω. Within our treatment, spin waves are the only excitations that contribute. Since they are not topological excitations and so do not carry net electrical charge, the dissipative conductivity vanishes in the low-frequency limit. Spin waves do, however, give rise to local charge fluctuations and a fluctuating electric dipole moment which couples to an oscillating external electric field, generating dissipation at finite frequency.

For a fully polarized quantum Hall ferromagnet, Green[20] has shown that the spin-wave contribution to optical conductivity is very small. In the noncollinear quantum Hall spin glass, the contribution may be larger due to the presence of a finite charge density in the disordered ground state. Furthermore, the low-energy dynamics of the collinear quantum Hall ferromagnet is qualitatively different from that of a quantum Hall spin glass, since while spin waves in a collinear background have a quadratic energy dispersion, those in a noncollinear background have a linear dispersion,[21] $\omega = cq$ at small q, with velocity

$$c = (\rho_s/\chi)^{1/2}. \tag{29}$$

Of the three polarization modes, one is expected to remain gapless even in the presence of a Zeeman coupling.

We now calculate the spin-wave contribution to the optical conductivity for a ground state with noncollinear spins, and then estimate its magnitude in realistic systems. The rotation of spins from their ground-state orientation in the presence of a spin wave may be parametrized by a vector $\vec{p}(\mathbf{r})$, with, at first order,

$$\vec{S} \to \vec{S} - \vec{p}(\mathbf{r}) \times \vec{S}. \tag{30}$$

Using Eq. (3), we show in Appendix A that this induces a change in the electron density

$$\delta\rho(\mathbf{r}) \to \delta\rho(\mathbf{r}) - \frac{\epsilon_{ij}}{4\pi} \partial_i \vec{p} \cdot \partial_j \vec{S}. \tag{31}$$

This linear dependence on $\nabla \vec{p}$ should be contrasted with spin waves in a collinear ferromagnet, for which the density change is $O(|\nabla \vec{p}|^2)$.

To estimate the contribution to the conductivity, we note that a spin wave will couple to an external electric field through the net dipole moment $\mathbf{P}$ that it induces. The coupling appears in the Hamiltonian in the form

$$\delta H = -P_x \mathcal{E}_x \tag{32}$$

for an electric field $\mathcal{E}_x$ in the x direction. From Fermi's golden rule, the power $\Pi(\omega)$ absorbed from an oscillating electric field of frequency ω is

$$\Pi(\omega) = \frac{2\pi}{\hbar^2} \mathcal{E}_x^2 |\langle f|P_x|0\rangle|^2 \hbar\omega g(\omega), \tag{33}$$

where $|0\rangle$ is the ground state and $|f\rangle$ is a state with a single spin wave excited, of excitation energy $\hbar\omega$, and $g(\omega)$ is the spin-wave density of states in frequency. From Eq. (29), we have

$$g(\omega) = \frac{3\omega}{2\pi c^2} L_x L_y, \tag{34}$$

including three polarizations for a system with linear dimensions L_x and L_y.

We estimate for the matrix element appearing in Eq. (33) by considering the dipole moment induced by a spin wave. We start our discussion using the form taken by a spin-wave mode in the absence of ground-state disorder, $\vec{p}(\mathbf{r}) = \alpha \vec{p}_0 \cos(\mathbf{q}\cdot\mathbf{r})$, where $\vec{p}_0$ is a unit vector defining the axis of spin rotations and α specifies the amplitude. The charge density induced by an excitation of this type in a disordered ground state with spin-correlation length ξ has, from Eq. (31), a magnitude $\alpha q/\xi$. We expect this to fluctuate with a random sign over the length scale ξ. The spin wave therefore induces electric dipoles of magnitude $e\xi(q\xi\alpha)$ in each correlation area ξ^2. Averaging over a $L_x \times L_y$ system, we find

$$\langle P_x^2 \rangle \sim (e\xi^2 q\alpha)^2 \frac{L_x L_y}{\xi^2} \sim e^2\alpha^2 \left(\frac{\omega\xi}{c}\right)^2 L_x L_y, \tag{35}$$

where we have substituted $q = \omega/c$.

It remains to determine the amplitude α for a single quantum excitation. We show in Appendix B that

$$\langle \alpha^2 \rangle = \hbar/\chi\omega L_x L_y. \tag{36}$$

Combining factors and dropping numerical coefficients, the absorbed power is

$$\Pi(\omega) \sim \mathcal{E}_x^2 \frac{e^2\xi^2\chi}{\rho_s^2} \omega^3 L_x L_y. \tag{37}$$

This is an ohmic response, $\Pi/L_x L_y = \sigma\mathcal{E}_x^2/2$, with conductivity

$$\sigma(\omega) \sim \frac{e^2}{h}\left(\frac{\omega\xi}{c}\right)^2 \frac{\hbar\omega}{\rho_s}. \tag{38}$$

Let us estimate the magnitude of this spin-wave conductivity. In the spin-glass phase, we use our numerical results to estimate $\rho_s \simeq J/2$. Also, the numerical results for the lattice shows $\chi_{\rm latt}$ of the order of unity in units of l_B^2/J. The continuum magnetization is related to the lattice spins by $\vec{m} \leftrightarrow \vec{S}\hbar/l_B^2$. This means that the continuum susceptibility is $\chi \simeq \hbar^2/Jl_B^2$. Combining these factors, we have

$$\sigma(\omega) \sim \frac{e^2}{h}\left(\frac{\xi}{l_B}\right)^2 \left(\frac{\hbar\omega}{\rho_s}\right)^3. \tag{39}$$

Taking $\xi = 10 l_B$ and $J = 4$–8 K (correcting our earlier value[4]), we find for a frequency of 1 GHz, $\sigma(\omega) \approx (10^{-3}$–$10^{-4}) e^2/h$. Unfortunately, variable-range hopping[22] seems likely to mask this contribution to $\sigma(\omega)$.

VIII. SUMMARY AND DISCUSSION

We have investigated the competition between exchange interactions and disorder in quantum Hall ferromagnets at or near integer filling and at zero temperature. Our approach is tailored to the limit of a smoothly varying impurity potential.

We find that the ferromagnetic state is destroyed by strong disorder through the creation of skyrmion/antiskyrmion pairs, or by a finite density of either skyrmions or antiskyrmions at filling factors sufficiently far from $\nu = 1$. This behavior, anticipated from simple scaling arguments, is confirmed in numerical studies of ground-state spin configurations, obtained from slow Monte Carlo cooling of an initially random high-temperature phase. The disordered phase is identified as a quantum Hall spin glass by the absence of long-range order, the presence of nonvanishing local magnetic moments, and a finite spin stiffness.

The quantum Hall spin glass has a zero-frequency dielectric response which interpolates between that of an insulator at small wave vectors, and that of a metal at large wave vectors. It supports gapless spin-wave modes that couple to electric fields through a finite dipole moment and contribute to the optical conductivity of the system.

Possible experimental signatures of the phenomena we have discussed follow both from the behavior of the magnetization and from the nature of excitations. Measurements of the Knight shift in nuclear magnetic resonance[23,24] (NMR) provide information on the distribution, sampled in space, of the spin-polarization component parallel to the applied magnetic field, while polarization-resolved absorption spectroscopy[25,26] can be used to determine the average spin polarization. Impurity effects are most characteristic at $\nu = 1$, where they result in a reduced spin polarization, reaching zero in the spin glass at zero Zeeman coupling, and a finite width in the polarization distribution. We note that spin polarization which remains unsaturated even at $\nu = 1$ is found in absorption spectroscopy,[25,26] and that a broad Knight-shift distribution is measured in low-temperature NMR.[24] In addition, the existence of excitations at energies lower than the Zeeman gap is characteristic of the partially polarized ferromagnet, and has been advanced as an explanation for a coupling observed in NMR experiments between radio-frequency magnetic fields and the electron system.[27] On the other hand, at filling factors away from $\nu = 1$, neither local probes nor the nature of excitations distinguish sharply between a skyrme crystal in a clean system and the partially polarized ferromagnet or spin glass induced by disorder.

ACKNOWLEDGMENTS

We are grateful for discussions with N. R. Cooper and S. L. Sondhi. The work was supported in part by the EPSRC under Grant No. GR/J78327 (J.T.C.) and by the Royal Society (D.K.K.L).

APPENDIX A: SPIN WAVES AND CHARGE FLUCTUATIONS

Consider a small rotation $\mathsf{R}(\vec{p})$ of the spins around $\vec{p}$, so that spin directions transform according to $\vec{S} \to \mathsf{R}\vec{S}$, with

$$\mathsf{R} = e^{\mathsf{P}}, \quad [\mathsf{P}]^{ab} = \epsilon^{abc} p^c. \tag{A1}$$

To second order, $\delta\vec{S} \simeq -\vec{p}\times\vec{S} + \vec{p}\times(\vec{p}\times\vec{S})/2$. The charge-density deviation from $\nu = 1$ is given by $\delta\rho_0 = \epsilon_{ij}\vec{S}\cdot(\partial_i\vec{S}\times\partial_j\vec{S})/8\pi$. In the presence of an additional spin rotation, it becomes

$$\delta\rho_0 + \delta\rho_1 = \frac{\epsilon_{ij}}{8\pi}\mathsf{R}\vec{S}\cdot[\partial_i(\mathsf{R}\vec{S})\times\partial_j(\mathsf{R}\vec{S})] \tag{A2}$$

so that

$$\delta\rho_1 = -\frac{\epsilon_{ij}}{4\pi}\partial_i\vec{p}\cdot\partial_j\vec{S} + \frac{\epsilon_{ij}}{8\pi}\partial_i\vec{p}\cdot\partial_j(\vec{p}\times\vec{S}) + O(p^3), \tag{A3}$$

obtained using $(\mathsf{R}^{-1}\partial_i\mathsf{R})\vec{S} \simeq (\partial_i\mathsf{P} - [\mathsf{P}, \partial_i\mathsf{P}]/2)\vec{S} = \vec{S}\times\partial_i\vec{p} + (\partial_i\vec{p}\times\vec{p})\times\vec{S}/2$. We can drop higher-order terms if $|\vec{p}| \ll 1$ and $|\nabla\vec{p}| \ll |\nabla\vec{S}|$, so that $\delta\rho_1/\delta\rho_0 \ll 1$.

To first order in p, the component of $\vec{p}$ parallel to $\vec{S}$ does not affect the charge density. At this order, the charge fluctuation $\delta\rho_1$ can be written as

$$\delta\rho_1 = -\epsilon_{ij}\partial_i\vec{p}\cdot\partial_j\vec{S}. \tag{A4}$$

From continuity, $\delta\dot{\rho}_1 + \partial_i J_i = 0$, the current density is

$$J_i = \epsilon_{ij}\dot{\vec{p}}\cdot\partial_j\vec{S} \quad + \text{divergence-free part.} \tag{A5}$$

Note that we have only identified the transport current, and not any circulating current in the bulk.

Let us now consider the energy cost of spin rotations for the Hamiltonian in Eq. (4). The change in the exchange energy density H_J is

$$\delta H_J = J\partial_i\vec{p}\cdot(\partial_i\vec{S}\times\vec{S}) + \delta H_J^{(2)},$$

$$\delta H_J^{(2)} = \frac{J}{2}[|\nabla \vec{p}|^2 - 2(\nabla \vec{p}\cdot\vec{S})^2 + (\partial_i \vec{p}\cdot\vec{S})\partial_i(\vec{p}\cdot\vec{S}) - (\vec{p}\cdot\vec{S})(\partial_i\vec{p}\cdot\partial_i\vec{S})]. \quad \text{(A6)}$$

The change in potential-energy density is

$$\delta H_\rho = V_{\rm H}(\mathbf{r})\,\delta\rho_1(\mathbf{r}) + \frac{1}{2}\int \delta\rho_1(\mathbf{r})U(\mathbf{r}-\mathbf{r}')\,\delta\rho_1(\mathbf{r}')d^2\mathbf{r}', \quad \text{(A7)}$$

where

$$V_{\rm H}(\mathbf{r}) = V(\mathbf{r}) - \mu + \int U(\mathbf{r}-\mathbf{r}')\,\delta\rho_0(\mathbf{r}')d^2\mathbf{r}' \quad \text{(A8)}$$

is the local Hartree potential and μ is the chemical potential.

An equation satisfied by the spin configuration in the ground state is obtained from requiring that the total energy is unaffected by the rotation $\vec{p}$ to first order. This means that we have to balance the first-order terms in the expressions for δH_J and δH_ρ, giving

$$\partial_i[J\partial_i\vec{S}\times\vec{S} - \epsilon_{ij}V_{\rm H}(\mathbf{r})\partial_j\vec{S}] = 0 \quad \text{(A9)}$$

for the spins in the ground state. This nonlinear equation demonstrates the competition between ferromagnetic exchange and Thomas-Fermi screening in a disordered QHFM.

From the second-order contributions $\delta H_J^{(2)}$ in the exchange energy δH_J, we can make a variational estimate of the spin stiffness in the spin-disordered phase. Suppose that $\vec{p}$ and $\vec{S}$ are uncorrelated. Then the second-order terms average to

$$\langle(\nabla\vec{p}\cdot\vec{S})^2\rangle = \langle(\partial_i\vec{p}\cdot\vec{S})\partial_i(\vec{p}\cdot\vec{S})\rangle = \frac{1}{3}|\nabla\vec{p}|^2,$$

$$\langle(\vec{p}\cdot\vec{S})(\partial_i\vec{p}\cdot\partial_i\vec{S})\rangle = 0. \quad \text{(A10)}$$

We can define a disorder-averaged spin stiffness from $\langle\delta H_J^{(2)}\rangle = \tilde{\rho}_s|\nabla\vec{p}|^2/2$ so that

$$\tilde{\rho}_s = 2J/3. \quad \text{(A11)}$$

APPENDIX B: LONG-WAVELENGTH SPIN WAVES

In this Appendix, we review the results of Halperin and Saslow[21] for hydrodynamic excitations, and of Ginzburg[28] for elementary excitations, and adapt these for our purposes. Both theories deal with long-wavelength, low-energy excitations of a disordered spin system. The microscopic magnetization density and energy density can be coarse grained over areas A to mean values; in the case of the magnetization one has

$$\vec{m}(\mathbf{r}) = \frac{1}{A}\sum_{i\in A}\vec{S}_i. \quad \text{(B1)}$$

Within a hydrodynamic theory, the low-energy dynamics of the system is determined entirely from these coarse-grained quantities, which obey conservation laws and are assumed to fluctuate slowly on the time scale set by local relaxation rates.

Hydrodynamic spin fluctuations have equations of motion which may be written in terms of the rotation angle $\vec{p}$, as used in Eq. (30), and the local magnetization, with the form

$$\frac{\partial p_\alpha}{\partial t} = \chi^{-1}m_\alpha, \quad \text{(B2)}$$

$$\frac{\partial m_\alpha}{\partial t} = \rho_s\nabla^2 p_\alpha, \quad \text{(B3)}$$

where ρ_s is the spin stiffness and χ is the uniform magnetic susceptibility. Using the same variables, the free energy of the system is

$$\Delta F(\vec{m},\vec{p}) = \frac{1}{2}\sum_{\alpha=1}^{3}\int d^2r\left(\frac{1}{\chi}m_\alpha^2 + \rho_s\left|\nabla p_\alpha\right|^2\right) = \frac{1}{2}\sum_{\alpha=1}^{3}\int d^2r(\chi\dot{p}_\alpha^2 + \rho_s|\nabla p_\alpha|^2). \quad \text{(B4)}$$

A long-wavelength treatment of elementary excitations leads to the same equations of motion and an equivalent expression for the energy of the system, in which ρ_s and χ are ground-state quantities. We have argued in Sec. V that both are finite at zero temperature in the spin-glass phase. These equations are reminiscent of the dynamics of the spin waves in a Heisenberg antiferromagnet. They lead to spin waves with the dispersion relation

$$\omega = cq; \quad c = (\rho_s/\chi)^{1/2}. \quad \text{(B5)}$$

Considering a single spin-wave mode, with

$$\vec{p} = \alpha\vec{p}_0\cos(\mathbf{q}\cdot\mathbf{r} - \omega t) \quad (|\vec{p}_0| = 1), \quad \text{(B6)}$$

we obtain the amplitude α for one quantum by setting the energy to $\hbar\omega$, arriving at Eq. (36).

APPENDIX C: DILUTE SKYRMIONS

In this Appendix, we study in more detail the interactions between a dilute set of skyrmions at weak disorder. We show how the relative orientations of internal degrees of freedom of the skyrmions are determined by the energetics of the system.

For a clean system without Hartree interactions, the Hamiltonian reduces to the $O(3)$ nonlinear sigma model. The skyrmions are of the Belavin-Polykov type. They do not interact. Hartree interactions alone will lead to a divergent skyrmion size in the absence of a Zeeman field. This is prevented in the presence of a disordered potential, as pointed out in Sec. III. However, the presence of an inhomogeneous potential also means that the skyrmions interact. We discuss here whether a physical picture of isolated skyrmions at weak disorder is justified. In particular, since the spin deviation due to a skyrmion falls off as $1/r$ with distance r, one must ask whether the ferromagnetic polarization is strongly

affected by a collection of dilute skyrmions.

For the purposes of this Appendix, we choose a simple disorder distribution in which pinned skyrmions and antiskyrmions are nucleated by isolated wells and barriers of circular shape, positioned randomly on the plane. The depth (or height) of these potentials exceeds the threshold, Eq. (9), so that they nucleate skyrmions (or antiskyrmions). This model disorder distribution has the advantage that we can use the Belavin-Polyakov solutions of the nonlinear sigma model as a starting point for our analysis.

Consider first the case in which the chemical potential is sufficiently high that there are no antiskyrmions. A set of Belavin-Polyakov skyrmions is described by an analytic function $w(z)$ of the position $z=x+iy$ in the plane

$$w(z)=\prod_{i=1}^{n}\frac{z-a_i}{z-b_i}, \tag{C1}$$

where n is the number of skyrmions. The function $w(z)$ parametrizes the spin configuration via

$$S_x+iS_y=2w/(1+|w|^2),$$

$$S_z=(1-|w|^2)/(1+|w|^2) \tag{C2}$$

with the boundary condition $S_x=1$ at infinity. For a single skyrmion ($n=1$), the density profile is

$$\delta\rho_{n=1}(z)\equiv\frac{|\partial_z w|^2}{\pi(1+|w|^2)^2}=\frac{d_i^2/4\pi}{(|z-z_i|^2+d_i^2/4)^2}, \tag{C3}$$

where $z_i=(a_i+b_i)/2$ can be interpreted as the position of the skyrmion and $d_i=|a_i-b_i|$ as its diameter. There remains an internal phase degree of freedom ϕ_i, defined from $(a_i-b_i)=d_i\exp(i\phi_i)$. In multiple skyrmion configurations the relative phases are important.

In a dilute glass, skyrmions are typically separated by distances large compared to their size, and the position and diameter of each skyrmion is determined separately by the balance of Hartree and potential energies in the vicinity of the potential well on which it is centered. In the region far from any well, the Belavin-Polyakov form is a good description for the spin configuration, because it minimizes exchange energy. The parameters z_i and d_i are fixed by the spin configuration within the ith well, while the values of ϕ_i remain to be determined. The density profile in this region is

$$\delta\rho'(z)=\frac{|w|^2}{\pi(1+|w|^2)^2}\left|\sum_i\frac{a_i-b_i}{(z-a_i)(z-b_i)}\right|^2, \tag{C4}$$

where the prime indicates the restricted area in which this form applies. The interference terms in the squared sum make a contribution to the total charge in the region far from the wells which amounts to a pairwise coupling between the internal degrees of freedom of different skyrmions. The integrated density is

$$I=\int{}'\frac{d^2z}{\pi}\frac{|w|^2}{(1+|w|^2)^2}\times\mathrm{Re}\sum_{i\neq j}\frac{(a_i-b_i)^*(a_j-b_j)}{(z^*-a_i^*)(z^*-b_i^*)(z-a_j)(z-b_j)}. \tag{C5}$$

In the dilute limit, we can take $a_i\simeq b_i=z_i$. We can also approximate $|w|^2\simeq 1$ away from the skyrmions. Then

$$I\simeq\mathrm{Re}\int{}'\frac{d^2z}{4\pi}\sum_{i\neq j}\frac{d_i d_j e^{i(\phi_i-\phi_j)}}{(z^*-z_i^*)^2(z-z_j)^2}=\frac{1}{2}\sum_{i>j}\frac{d_i d_j\cos(\phi_i-\phi_j)}{|z_i-z_j|^2}. \tag{C6}$$

This contribution to the charge in the region between potential wells adds to the energy of the system, since the electrostatic potential here does not exceed threshold [Eq. (9)]. It represents charge density that is removed from the cores of skyrmions, as a result of overlap with the tails of other distant skyrmions. We see that in order to minimize the energy we must choose the skyrmion phases ϕ_i to minimize I. This is done by arranging ϕ_i so that the variable $d_i e^{i\phi_i}$ sums locally to small values. With such correlations, we expect that long-range ferromagnetic order survives in the presence of dilute skyrmions. A similar treatment of a mixed system containing both skyrmions and antiskyrmions leads to interactions of the same kind among the skyrmions, and separately among the antiskyrmions, but without coupling between the two species at leading order in inverse density.

[1] S. M. Girvin, *Ecole des Houches: Topological Aspects of Low Dimensional Systems* (Les Editions de Physique, Paris, 1999).

[2] S. L. Sondhi, A. Karlhede, S. A. Kivelson, and E. H. Rezayi, Phys. Rev. B **47**, 16 419 (1993).

[3] R. Rajaraman, *Solitons and Instantons* (North-Holland, Amsterdam, 1989).

[4] S. Rapsch, J. T. Chalker, and D. K. K. Lee, Phys. Rev. Lett. **88**, 036801 (2002).

[5] M. M. Fogler and B. I. Shklovskii, Phys. Rev. B **52**, 17 366 (1995).

[6] T. Ando and Y. Uemura, J. Phys. Soc. Jpn. **35**, 1456 (1973).

[7] M. A. Paalanen, D. C. Tsui, B. J. F. Lin, and A. C. Gossard, Phys. Rev. B **25**, 5566 (1982).

[8] D. R. Leadley *et al.*, Phys. Rev. B **58**, 13 036 (1998).

[9] A. G. Green, Phys. Rev. B **57**, 9373 (1998).

[10] A. J. Nederveen and Y. V. Nazarov, Phys. Rev. Lett. **82**, 406 (1999).

[11] J. Sinova, A. H. MacDonald, and S. M. Girvin, Phys. Rev. B **62**, 13 579 (2000).

[12] G. Murthy, Phys. Rev. B **64**, 241309 (2001).

[13] A. L. Efros, Solid State Commun. **65**, 1281 (1988).

[14] A. L. Efros, Solid State Commun. **70**, 253 (1989).

[15] K. Moon, H. Mori, K. Yang, S. M. Girvin, A. H. MacDonald, L. Zheng, D. Yoshioka, and S.-C. Zhang, Phys. Rev. B **51**, 5138 (1995).
[16] N. Read and S. Sachdev, Phys. Rev. Lett. **75**, 3509 (1995).
[17] C. Timm, S. M. Girvin, P. Henelius, and A. W. Sandvik, Phys. Rev. B **58**, 1464 (1998).
[18] M. Hale, O. Schwindt, and T. Weidig, Phys. Rev. E **62**, 4333 (2000).
[19] A. B. Harris, J. Phys. C **7**, 1671 (1974).
[20] A. G. Green, Phys. Rev. Lett. **82**, 5104 (1999).
[21] B. I. Halperin and W. M. Saslow, Phys. Rev. B **16**, 2154 (1977).
[22] D. G. Polyakov and B. Shklovskii, Phys. Rev. B **48**, 11 167 (1993).
[23] S. Barrett, G. Dabbagh, L. Pfeiffer, K. West, and R. Tycko, Phys. Rev. Lett. **74**, 5112 (1995).
[24] P. Khandelwal, A. E. Dementyev, N. N. Kuzma, S. E. Barrett, L. N. Pfeiffer, and K. W. West, Phys. Rev. Lett. **86**, 5353 (2001).
[25] E. H. Aifer, B. B. Goldberg, and D. A. Broido, Phys. Rev. Lett. **76**, 680 (1996).
[26] V. Zhitomirsky, R. Chughtai, R. J. Nicholas, and M. Henini, Physica E (Amsterdam) **12**, 12 (2002).
[27] N. N. Kuzma, P. Khandelwal, S. E. Barrett, L. N. Pfeiffer, and K. W. West, Science (Washington, DC, U.S.) **281**, 686 (1998).
[28] S. L. Ginzburg, Zh. Éksp. Teor. Fiz. **75**, 1497 (1978) [Sov. Phys. JETP **48**, 756 (1978)].